SMALL MOLECULE INHIBITORS OF THE SARS-COV NSP15 ENDORIBONUCLEASE, MECHANISM OF ACTION AND INSIGHT INTO CORONAVIRUS INFECTION

A Thesis

by

JOANNA MARIA ORTIZ ALCANTARA

Submitted to the Office of Graduate Studies of
Texas A&M University
in partial fulfillment of the requirements for the degree of

MASTER OF SCIENCE

May 2009

Major Subject: Biochemistry

SMALL MOLECULE INHIBITORS OF THE SARS-COV NSP15 ENDORIBONUCLEASE, MECHANISM OF ACTION AND INSIGHT INTO CORONAVIRUS INFECTION

A Thesis

by

JOANNA MARIA ORTIZ ALCANTARA

Submitted to the Office of Graduate Studies of
Texas A&M University
in partial fulfillment of the requirements for the degree of

MASTER OF SCIENCE

Approved by:

Chair of Committee,	Cheng C. Kao
Committee Members,	Andreas K. H. Holzenburg
	Julian L. Leibowitz
	Ryland F. Young
Head of Department,	Gregory D. Reinhart

May 2009

Major Subject: Biochemistry

ABSTRACT

Small Molecule Inhibitors of the SARS-CoV Nsp15 Endoribonuclease, Mechanism of Action and Insight into Coronavirus Infection. (May 2009)

Joanna Maria Ortiz Alcantara, B.S., National Autonomous University of Mexico

Chair of Advisory Committee: Dr. Cheng C. Kao

The Severe Acute Respiratory Syndrome (SARS) virus encodes several unusual RNA processing enzymes, including Nsp15, an endoribonuclease that preferentially cleaves 3' of uridylates through a Ribonuclease A-like mechanism. Crystal structures of Nsp15 confirmed that the Nsp15 active site is structurally similar to that of Ribonuclease A. These similarities and our molecular docking analysis lead us to hypothesize that previously characterized Ribonuclease A inhibitors will also inhibit the SARS-CoV Nsp15. Benzopurpurin B, C-467929, C-473872, N-36711, N-65828, N-103018 and Congo red were tested for effects on Nsp15 endoribonuclease activity. A real-time fluorescence assay revealed that the IC_{50} values for inhibiting Nsp15 were between 0.2 μM and 40 μM. Benzopurpurin B, C-473872, and Congo red are competitive inhibitors, according to kinetic studies and were demonstrated to bind SARS-CoV Nsp15 by a differential scanning fluorimetry assay. Benzopurpurin B also inhibited the Nsp15 orthologs from two other coronaviruses: mouse hepatitis virus (MHV) and infectious bronchitis virus. The three compounds reduced infectivity of MHV in L2 cells by 8 to 26 fold. The more effective drugs also caused a decrease in MHV RNA accumulation.

DEDICATION

To my Mom and Dad, Cecilia and Bernardo, for their love, guidance and support, for their encouragement to be better everyday and for their wise words.

To my sisters, Ivette and Nelly for being such good friends and for their geniality, for all the good times we spend together.

To Hector, for being the light of my life, making everyday so shiny, because with you around everything makes sense and there is always hope, for sharing with me all those laughs and tears, for all the moments you were here and you were not and for being so patient. I love you.

ACKNOWLEDGEMENTS

I would like to thank my committee chair, Dr. Kao, and my committee members, Dr. Holzenburg, Dr. Leibowitz, and Dr. Young, for their support and guidance throughout the course of this research.

I extend my gratitude to my colleagues at Texas A & M University, specially Kanchan Bhardwaj, Satheesh Palaninathan, Lillian Li Yi and Will Snee and everybody in Kao's lab who were willing to share their knowledge and experience to support my research. I extend my gratitude to the Biochemistry & Biophysics faculty and staff for making my time here a great and rich experience. I also gratefully acknowledge a National Science Foundation supplemental grant to develop the differential fluorimetry assay, and the NIAID which partially provided the funding for this research.

Thanks to my mom, dad and sisters for their encouragement, to Hector for his patience and love and Adriana Perea, Catalina Velez and Hermes Reyes for their friendship.

NOMENCLATURE

SARS-CoV	Severe Acute Respiratory Syndrome Coronavirus
Nsp15	Nonstructural Protein 15
RNase A	Ribonuclease A
MHV	Mouse Hepatitis Virus
IBV	Infectious Bronchitis Virus

TABLE OF CONTENTS

Page

LIST OF FIGURES

INTRODUCTION

The Severe Acute Respiratory Syndrome (SARS) outbreak emerged in Southeastern China in 2002 and eventually spread to 30 countries by 2003. SARS was characterized by an atypical pneumonia transmitted primarily by contact with infectious respiratory droplets or fomites and it was responsible for 8096 confirmed cases with a mortality rate of about 10% (WHO). SARS is caused by the SARS coronavirus (SARS-CoV) (1, 2, 3). Horseshoe bats are the natural reservoir of SARS-CoV like viruses but they have been isolated also from palm civets and raccoon dogs from wild animal markets in China, suggesting that these mammals served as an amplification host and could be the source of infection in humans (4, 5, 6). The existence of a natural reservoir raises the possibility of a reemergence of SARS. The treatment used during the epidemic consisted of corticoid steroids and ribavirin (1, 2, 3). In hindsight, some of these treatments had severe side effects and minimal efficacy (1, 2, 3). Currently there are no approved anti-virals against SARS (7), and specific therapeutic options will be needed to contain future outbreaks.

SARS is a member of the group II *Coronavirus* within the order *Nidovirales* (8). Coronaviruses are enveloped and their positive-strand RNA genomes are the largest known, they are of interest in their mechanism of gene expression and replication. In this section, a general overview of the biology of coronaviruses will be presented, from their

---

This thesis follows the style of *The Journal of Biological Chemistry.*

taxonomy, morphology and genome organization to their viral replication cycle, including a summary of the proposed RNA synthesis and processing mechanisms and the proteins involved (for reviews of coronaviruses, see references 9-11).

Biology of Coronavirus Infection

Taxonomy

The *Coronaviridae* family of enveloped RNA viruses is formed by two genera, the coronaviruses and the toroviruses, which together with the arteriviruses and roniviruses form the order *Nidovirales.* Members of the coronavirus family are divided in three groups, originally based on antigenic relationships, later by comparisons of the sequences of the entire viral genomes (12). Coronaviruses cause respiratory or intestinal infections. Most of the group 1 and group 2 coronaviruses infect mammals, and human coronaviruses are classified in these groups. Group 3 viruses have avian hosts only. Mouse hepatitis virus (MHV), human coronavirus OC43, and the bovine coronavirus are members of group 2, of which SARS-CoV according to rooted phylogenetic trees together with bat SARS-CoV form group 2b, and the infectious bronchitis virus is member of group 3 (8, 13).

Virion morphology

Coronaviruses are spherical, with virions of about 80-120 nm projecting club-like, petal shaped surface spikes of 17-20 nm from the lipid envelope, and helical nucleocapsids according to negatively stained electron micrographs (14, 15).

Genome organization

Coronaviruses have nonsegmented, single-stranded positive RNA genomes of about 30 kb, with 5' caps and 3' poly(A) tails; the largest among all RNA viruses. The SARS-CoV genome contains ~29730 nucleotides excluding the 3' poly(A) tail. The 5' and the 3' untranslated regions contain 265 and 342 nucleotides respectively. The genome is predicted to have 14 functional open reading frames (ORFs). Two large, 5'-terminal ORFs 1a and 1b form the replicase gene that encodes 16 nonstructural proteins including those required for viral RNA synthesis. The other twelve ORFs encode the structural proteins S, M, N and E and eight accessory proteins (16, 17, 18).

Viral replication cycle and virion assembly

Coronaviruses entry into target cells initiate with binding of the viral S (Spike) protein to cellular receptors. Trimers of the Spike protein decorate the virion surface like the spikes in a crown and inspired the name for this group of viruses. The Spike protein is heavily glycosylated and have three domains, the N-terminal S1, which is conserved and the C-terminal transmembrane and cytoplasmic S2 subdomains. The minimal binding domain of the SARS-CoV S protein was mapped to the residues 318-510 of S1 and antibodies specific for this subunit neutralize SARS-CoV infection (19, 20). Aminopeptidase N, a zinc metalloprotease is the receptor of several group 1 coronaviruses (21); carcinoembryonic antigen-related cell adhesion molecules are cellular receptors of MHV from group 2 (22) and the angiotensin-converting enzyme 2 (ACE2), a metalloprotease expressed in the lung, intestine, liver, heart, vascular

endothelium, testis and kidney is the functional cellular receptor of SARS-CoV (23, 24). S1 binds to the cellular receptor triggering conformational changes that will co-localize the fusion peptide upstream of the two heptad repeats of S2 to the transmembrane domain to facilitate fusion of the viral and cellular membranes. SARS-CoV membrane fusion is activated within endosomes by cathepsin L proteolysis (25, 26).

Following the fusion, the viral genome RNA is released into the cytoplasm of the infected cell, the mechanism involved in the RNA uncoating is not well understood. Genome expression of the SARS-CoV starts with the cap-dependent translation of the genomic RNA, mRNA 1, producing a 4382 amino-acid protein called polyprotein 1 (pp1a) encoded by ORF 1a; then the 7073-residue polyprotein 1ab (pp1ab) encoded by ORFs 1a and b sequences is produced by ribosomal frameshifting. This occurs into the -1 reading frame, just upstream of the ORF1a translation stop codon mediated by the signal of the slippery sequence ^{13392}UUUAAAC^{13398} and a downstream RNA pseudoknot structure. Polyproteins pp1a and pp1ab are processed by viral proteinases into Nsp1-16 to form the viral replicase-transcriptase multi-protein complex. In general, coronaviruses process the replicative polyproteins at the N-proximal regions at three sites using two papain-like proteases PL1^{pro} and PL2^{pro}. SARS-CoV uses only one papain-like protease, a PL2^{pro} orthologue with narrow substrate specificity, containing a putative Zn-finger structure required for the proteolytic activity (18, 27, 28). The central and C-terminal regions of pp1a and pp1b are processed by the chymotrypsin-like protease 3CL ^{pro}, also called the coronavirus main protease, M^{pro} , that releases the RdRp and helicase, key

replicative functions. The SARS-CoV 3CL ^{pro} cleaves pp1a and pp1ab at 11 sites, as illustrated in Fig. 1 (18, 29, 30).

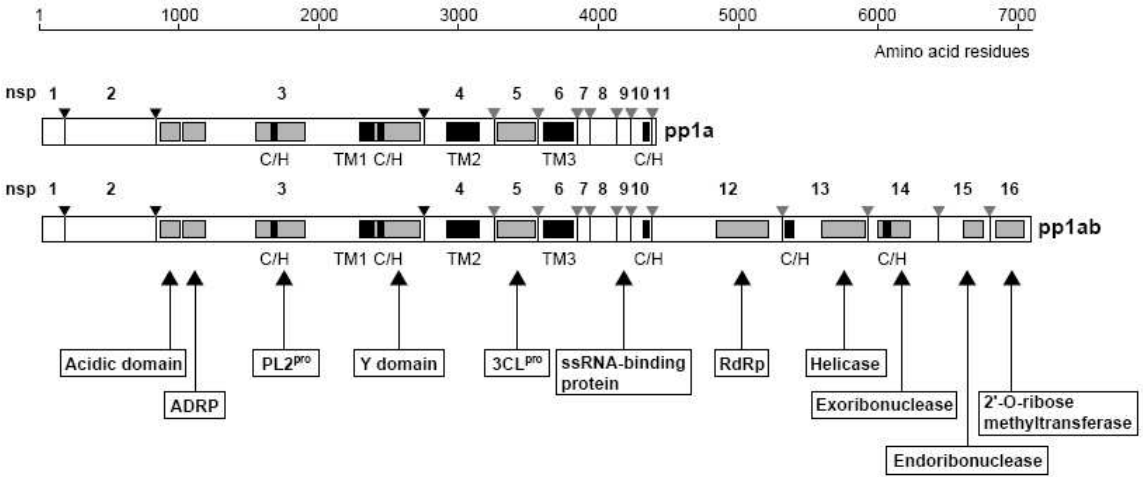

FIGURE 1. **Domain organization and proteolytic processing of SARS-CoV replicase proteins.** Taken from Ziehbur J. (2004) *Curr. Opin. Microbiol.* (31).

The viral replicase-transcriptase complex mediates the viral genome replication and the transcription of a nested set of eight subgenomic (sg) mRNAs, both require the synthesis of negative-strand intermediates. All the sg mRNAs have a 72-nucleotide, 5'-terminal leader sequence identical to the 5'-end of the genome, and they are generated by discontinuous synthesis rather than full-length RNA transcription as supported by UV transcription mapping experiments in MHV-infected cells in which the size of a given mRNA was correlated to the target size for ultraviolet light irradiation for the synthesis of that mRNA (32) and principally by mixed infection experiments, in which the

reassortment of leader sequences was observed in the mRNAs produced in cells infected with two different strains of MHV (33). The discontinuous synthesis of RNA depends on transcription-regulating sequences TRSs, cis-active RNA elements with the common core sequence ACGAAC for the SARS-CoV (18). There is currently consensus in the field about discontinuous transcription occurring during the synthesis of minus RNA strands. In the leader-primed transcription model the leader RNA is produced first, then transferred to the full-length minus strand, to the complementary TRS (34). In a second model, the nascent minus strand synthesis is paused at the TRSs and translocated to the leader TRS located downstream of the 5'-leader sequence on the genomic RNA, to continue the transcription. The minus-strand RNAs containing the anti-leader sequence are then used as templates for continuous plus-strand synthesis of sg mRNAs (35, 36, 37). Complementary base-pairing and protein-protein interactions keep the 5' end of the genome close to the site of minus-strand synthesis in both models. The negative-strand discontinuous transcription model is currently gaining favored status (37). The finding in infected cells of subgenomic minus strand RNAs with antileader sequence, subgenomic replicative-intermediate RNAs active for transcription for each mRNA (38, 39, 40) as well as the analysis of RNA synthesis using equine arterivirus full-length infectious cDNA in which mutations were introduced in the leader or body copies of TRS performed support this model (41, 42, 43, 44). The SARS-CoV structural proteins S, M, N and E, and eight additional proteins with unknown functions are predicted to be encoded in RNAs 2-9. mRNAs 2, 4, 5 and 6 are functionally monocistronic, mRNAs 3, 7, 8 and 9 bicistronic, Fig. 2. (8, 18).

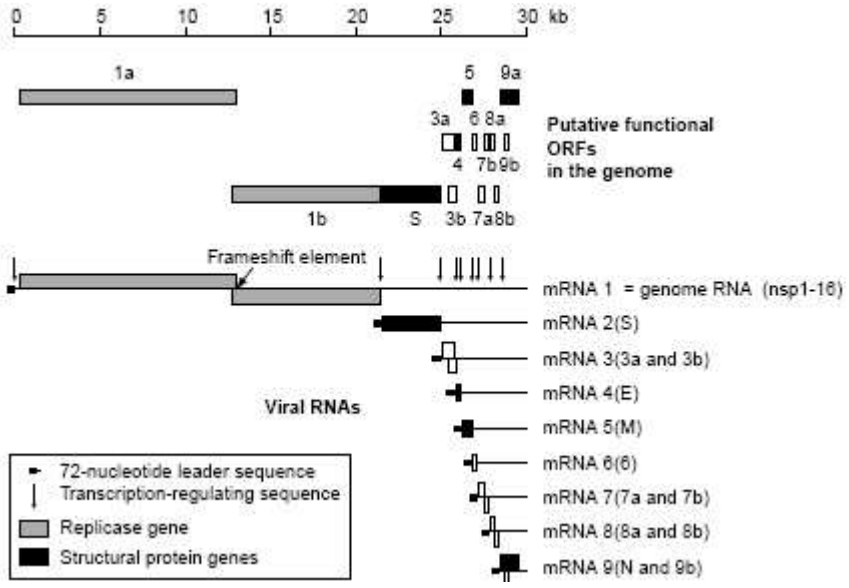

FIGURE 2. **Genome organization and RNA synthesis of SARS-CoV.** Taken from Ziehbur J. (2004) *Curr. Opin Microbiol.* (31).

Coronaviruses likely attach the replication machinery to the membrane of autophagosomes forming double-membrane vesicles (9). The membrane bound structural proteins M, S, and E are inserted into the endoplasmic reticulum ER, then they transit to the endoplasmic reticulum-Golgi intermediate compartment ERGIC. When viral genomic RNA and structural proteins are accumulated, the N protein, the most abundantly expressed viral protein, encapsidate the progeny genomes forming nucleocapsids that interact with the membrane-bound proteins and bud into the ERGIC to form virions. Progeny virions are transported to the plasma membrane in vesicles or Golgi sacs not yet clearly defined to be exported out of the infected cell (9).

Proteins involved in RNA synthesis and processing

The roles of many of the nonstructural proteins that assemble a membrane-associated replicase-transcriptase complex are not completely elucidated. However, several have novel functions that are not found in smaller positive-strand RNA viruses (8). Included in these are proteins Nsp8, a putative RNA primase for Nsp12, the RNA-dependent RNA polymerase; Nsp14, a 3' to 5' exoribonuclease that may serve proofreading functions; Nsp15, an endoribonuclease, and Nsp16 a putative methyltransferase that acts on the ribose 2' hydroxyl (45, 46, 47, 48).

Nsp12 is the coronavirus RNA-dependent RNA polymerase (RdRp), it is predicted to have the fingers, palm and thumb domains characteristic of other viral and reverse transcriptases, and unique to coronaviruses a very large amino-terminal domain essential for activity and containing the segment responsible for the association of the RdRp with intracellular membranes. RdRp has been shown to associate with M^{pro}, Nsp8 and Nsp9 (49, 50). Nsp8 is a putative second RdRp unique to coronaviruses with specificity for the internal 5'-(G/U)CC-3' trinucleotides on RNA templates to start the synthesis of complementary oligonucleotides of less than 6 nucleotides with low fidelity. It is proposed to produce primers for the Nsp12 RdRp (45). In this regard, Nsp8 is highly novel in acting as a RNA primase for a viral RNA-dependent RNA polymerase.

Nsp13 is a helicase with multiple activities according to studies in HCoV-229E and SARS-CoV. It binds single and double-stranded RNA and DNA. It has NTPase and dNTPase activities, that are template-dependent, probably to provide the energy to translocate along the template. It unwinds both DNA and RNA duplexes and is more

processive in a 5'-to-3' direction, suggesting a role in the preparation of the template for RNA synthesis by the RdRp complex. It has RNA 5'-triphosphatase activity, proposed to participate in the 5' cap synthesis on coronavirus RNA (51, 52, 53, 54).

Nsp14 has exoribonuclease activity. It has been shown to act on the 3' to 5' direction on single and double-stranded RNA and requires divalent metal ions for its activity. It does not hydrolyze ribose-2'-O-methylated RNA or DNA substrates. Its ribonucleolytic activity is regulated by binding to the dsRNA. It is involved in viral RNA synthesis. Active site mutants of the human CoV 229E Nsp14 are defective in viral sgRNA synthesis, they present reduced genome replication and no viable virus can be recovered (46).

Nsp15, the topic of this research, is an uridylate-specific endoribonuclease that will be described in detail later.

Nsp16 is a putative 2'-O-methyltransferase (2'-O-MT), activity that is speculated to participate in RNA capping or in negative-strand RNA synthesis (8, 48).

Nsp14-16, with ExoN, Nendo U and 2'-O-MT activities respectively are located in a single protein block in pp1ab just next to the RdRp and helicase, suggesting that they may have concerted activities. Snijder *et al.* (8) proposed a parallel to two cellular RNA processing pathways. In one of them, Xendo U and ExoN participate in the cleavage of pre-mRNA to produce U16 and U86 intron encode small nucleolar RNAs (snoRNAs) that could be used in subsequent rRNA processing mediated by 2'-O-methylation and the 2'-O-MT activity. In the second, an ADP-ribose 1''-phosphatase (ADRP) and a cyclic phosphodiesterase (CPD) present only in some group 2

coronaviruses but not SARS would be involved, in comparison to their cellular homologs that mediate the ADP-ribose 1', 2' cyclic phosphate processing to produce mature tRNA. However, the roles of the viral enzymes in a given pathway as well as their biological substrates are still elusive. It is interesting that although the ExoN, NendoU, 2'-O-MT and ADRP activities are conserved in all coronaviruses, just the NendoU is conserved in arteriviruses whose genomes are smaller, suggesting that given the extremely large genome of the coronaviruses, extra activities are required for RNA replication and transcription similar to DNA organisms but unprecedented for RNA viruses; as an example, it has been speculated that ExoN could have a role in RNA proofreading and repair, activities not seen in RNA viruses, as well as recombination. These predictions still need to be proved experimentally (8).

The SARS-CoV Nsp15 Endoribonuclease

This section will summarize the features of the SARS-CoV Nsp15, required for its enzymatic activity, and the structural properties required for oligomerization and substrate recognition.

Nsp15 has endoribonuclease activity. It cleaves at RNA uridylates, stimulated by Mn^{2+} as a cofactor, which could induce a conformational change in the protein according to measurement of changes in tryptophan fluorescence (47, 48). Later it was demonstrated that the cleavage occurs specifically at 3' of uridylates, preferentially unpaired, with higher affinity for substrates with consecutive uridylate bases, and in the proper sequence context it can also cleave 3' of cytidylates, and Mn^{2+} enhance RNA

binding (55). Upon cleavage of RNA molecules a 2'-3' cyclic phosphate ended molecule is produced (48, 55). It has been named Nendo U and it is a genetic marker of nidoviruses that is not present in other RNA viruses (8, 48). It has similarities to Xendo U, an endoribonuclease from *Xenopus laevis* that participates in the processing of pre-mRNA to produce small nucleolar RNAs. Xendo U is also uridylate-specific, Mn^{2+} dependent and generates products with 2'-3' cyclic phosphate ends; besides the functional aspects both endoribonucleases have sequence similarities (8, 56, 57). Nsp15 plays a role in viral replication and transcription as demonstrated in a study with a Human CoV 229E active site mutant in which viral RNA synthesis was abolished (48). Furthermore, in mutational studies in the Arterivirus Nsp15 ortholog, several active site mutants showed reduced plaque formation and virus titers (58). Similar observations were reported for MHV A59 (59). Nsp15 is not able to cleave 2'-O-ribose methylated RNA, suggesting a functional cooperation with Nsp14, a putative 2'-O-ribose methyltransferase. (48).

The WT SARS-CoV Nsp15 was found to be in equilibrium between monomers, trimers and hexamers in solution. Only the hexameric form is enzymatically active (60). Transmission electron microscopy demonstrated that Nsp15 assembles into a hexameric structure formed by a dimer of trimers interacting end-to end, forming a narrow tunnel in the center and several channels. It is also the hexameric form that binds to RNA. The RNA binding to the outside of the hexamer, interacting with both trimers, was suggested by a low-resolution co-crystal of Nsp15 and RNA (55, 60). Crystal structures with one subunit in the asymmetric unit have been solved for SARS-CoV Nsp15 and its MHV

ortholog (61, 62). Six catalytic sites are exposed at the surface when a hexamer is assembled. The three catalytic residues His-234, His-249, Lys-289 located in the C-terminal domain of the SARS-CoV Nsp15 resemble the catalytic triad His-12, Lys-41 and His-119 found in Ribonuclease A and although superimposition of tertiary structures was impossible, the catalytic residues Lys-His-His of both enzymes were superimposed successfully (61), supporting previous mutational studies in which the residues His-234, His-249, Lys-289 and Asp-272 of SARS-CoV Nsp15 (60), and the corresponding residues His-His-Lys in the MHV ortholog (62) were required for ribonucleolytic activity, proving to have a direct role in catalysis, as it was suggested because they are highly conserved among members of the Xendo U family and coronavirus orthologs (8). Furthermore, mechanistic similarities between RNase A and Nsp15 are also conceivable, in RNase A, His-12 and His-119 have general base and general acid functions, and the pentacovalent intermediate is stabilized by the interaction of the phosphate moiety with Lys-41. In SARS-Co-V Nsp15 the position of the two catalytic histidines suggest they can accept and donate protons, and this is supported by the fact that Nsp15 cannot cleave DNA or 2'-O-methylated RNA where there is no 2'-OH to be deprotonated by His-249; for both enzymes 2'-3' cyclic phosphate molecules are produced, see Fig. 3 (48, 55, 61, 63).

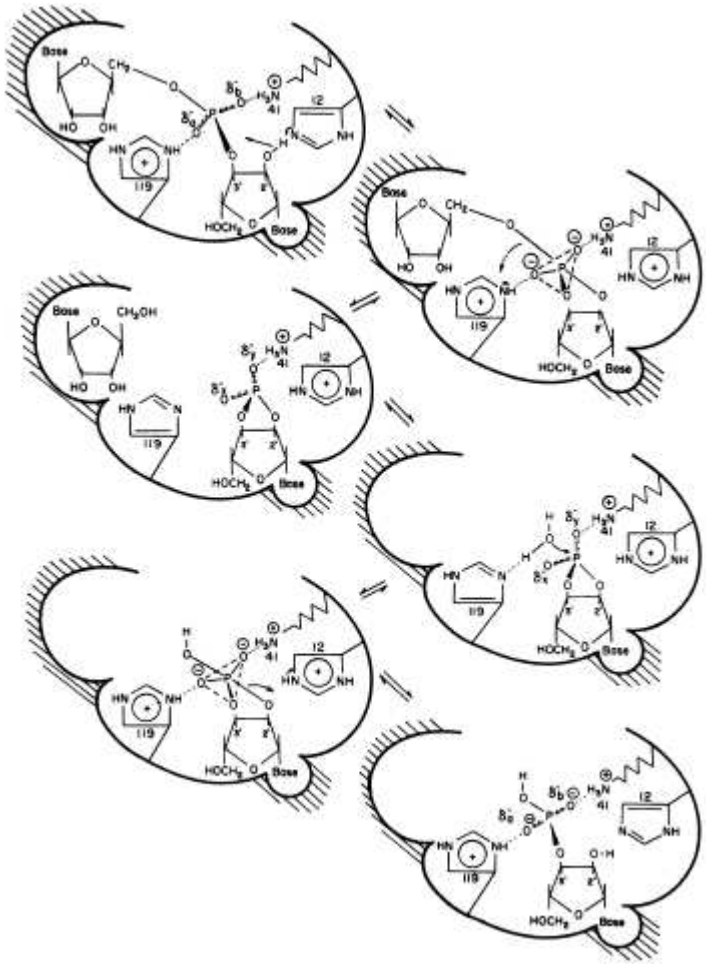

FIGURE 3. **Mechanism of action of Ribonuclease A.** Taken from Roberts G. *et al.* (1969) *PNAS* (63).

Of note the C-terminal tail of Nsp15 folds towards the active site suggesting that residues at that location could be important for substrate recognition and specificity (61).

The elucidation of the structure of a SARS-CoV active-site mutant with six subunits in the asymmetric unit led to the prediction of residues required for subunit interaction, specificity in substrate recognition and RNA binding (64). The N-terminal residue E3, previously demonstrated to be involved in oligomerization, plays a role in

trimer-trimer interactions according to the crystal structure (60, 64). Residues N52, I26 and I27, were also predicted to participate in trimer-trimer interactions. Interestingly, the mutants E3A, N52A, I26, 27A expected to form trimers eluted as monomers in gel filtration, suggesting that trimers are unstable intermediates. Consistent with hexamers being required for endoribonuclease activity, Nsp15 with mutations that prevented proper trimer-trimer interaction had endoribonuclease activity to less than 1% of WT. D39, R90, E266, participate in intratrimer interactions, and mutations in these residues in Nsp15 result in proteins that elute as monomers and show a significant reduction in endoribonuclease activity to less than 1% of WT. A N163A mutant, also expected to be affected on interactions between trimers, was found to form monomers and hexamers with nearly equal distribution, and to have 29% of the activity of WT (21). A molecular docking analysis with UMP revealed that some active site residues located in the C-terminal tail could play a role in specificity and substrate recognition. S293, Y342, L345 and P343 were predicted to be important. Previously Ricagno *et al.* (61) observed that superimposing RNase A and Nsp15 catalytic triads, the positions of S293 and Y342 of Nsp15 were comparable to those of T45 and F120 of RNase A that participate in pyrimidine specificity by forming hydrogen bonds and van der Waals interactions with the base respectively. In the docking model, S293 could form H-bonds with the uracil, and the aromatic ring of Y342 could stack against the uracil while P343 and L345 are above it narrowing the pocket. The catalytic residues K289, H234 and H249 are positioned to interact with the ribose 2' OH and the phosphodiester group as illustrated in Fig. 4 (64).

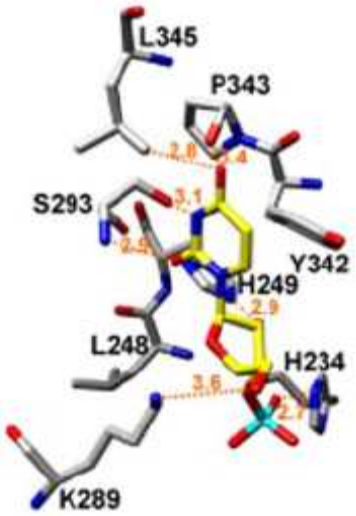

FIGURE 4. **Molecular docking of UMP into the Nsp15 active site.** Taken from Bhardwaj, et al. (2008) *J. Biol. Chem.* (64).

S293, L345, P343 and Y342 were demonstrated to be important for catalysis since Nsp15 mutants of this residues showed either a reduction in endoribonuclease activity in comparison to WT, or inactivity (Y342A), while no alterations in the oligomerization state were observed. The role of S293 in specificity was established in a study in which mutants to A, N or T were constructed. All the mutants formed hexamers. In this study, S293T showed very low cleavage activity against cytidylates and uridylates in comparison to WT, S293N cleaved cytidylates and uridylates with strong preference for uridylates comparable to WT, while S293A presented similar rates of cleavage of cytidylates and uridylates and was not able to cleave purines, demonstrating that this residue is important to specifically recognize the substrate (64). P343 and L345

are also important for substrate recognition according to observations made in mutants of these residues that would have a wider pocket or a more flexible active site. P343G was showed to have reduced catalytic activity in comparison to WT and preference to cleave uridylates over cytidylates. L345G had reduced cleavage activity, with nearly equal preference for uridylates and cytidylates and interestingly it was able to cleave purines, confirming that this residue should sterically block the access of a purine in the WT catalytic pocket (64). In the same study, mutants H18A, T47A,N28/29A, N73A and K256A presented decreased RNA binding as well as the active site mutants Y342A and L345G, suggesting that these residues contribute to RNA binding (64).

Ribonucleases are classified in two main groups. The ribonucleases in the first group include RNase H and RNase III, they depend on two metal ions, one to activate the substrate, the second to stabilize the transition state; they cleave 5' of the cognate phosphodiester. The second group formed by members of the RNase A family and RNase T1 are independent of metal ions and cleave at 3' of the cognate phosphodiester. Nsp15 shares characteristics of both groups, its activity is enhanced by Mn^{2+} and its mechanism of cleavage is similar to that of RNase A; it together with Xendo U define a novel family of endoribonucleases, endo U (65, 66, 67, 68).

Nendo U is a promising target for developing antiviral drugs, given that is widely conserved among nidoviruses but absent in other RNA viruses, and it plays an important role in viral RNA synthesis.

Compounds Benzopurpurin B, C-473872, C-467929, N-306711, N-103019 and N-65828 were previously described as inhibitors binding to the active site of angiogenin

and RNase A, by Kao, R. Y., *et al.* (69) and Jenkins, J. L., *et al.* (70). Congo red is an analog of Benzopurpurin B. The structural and mechanistic similarities between SARS-CoV Nsp15 and RNase A suggested that those compounds might inhibit the endoribonuclease activity of coronavirus Nsp15.

OBJECTIVES

The present study is intended to determine whether small-molecule inhibitors of RNase A and Angiogenin, an RNase A–like enzyme, can affect enzymatic activity of the SARS-CoV Nsp15 endoribonuclease (sNsp15) *in vitro* and coronavirus infection in cultured cells.

Specific aim 1: To investigate whether the selected small-molecule inhibitors of RNase A and Angiogenin are also able to inhibit the endoribonuclease activity sNsp15 and to establish their mechanism of inhibition. A real-time fluorescence assay was used to study the efficacy of the compounds on the activity of purified sNsp15 *in vitro*. A gel-based assay was used to confirm the results. To demonstrate binding of the compounds to sNsp15 differential scanning fluorimetry assays were performed. The mechanism of inhibition of the compounds was analyzed using kinetic studies.

Specific aim 2: To test the effects of the selected small-molecule compounds on Nsp15 orthologs of other coronaviruses. The activity of the compounds on highly purified recombinant MHV and IBV Nsp15 orthologs was established by the real-time fluorescence assay.

Specific aim 3: To examine the effect of the compounds on MHV infection in cultured cells and to investigate the effect of the compounds on viral RNA synthesis. Plaque assays were performed in L2 cells for MHV. Agarose gel electrophoresis of viral RNAs metabolically labeled in the presence of actinomycin D was used to study the effect of the compounds on the production of genomic and sub-genomic MHV RNAs.

MATERIALS AND METHODS

Reagents

SARS and MHV Nsp15 His-tagged at the N termini, and IBV Nsp15 with an His-tag at both termini were expressed in *E. coli* and purified by metal ion affinity chromatography and Mono Q ion exchange chromatography as previously described (47). The proteins were stored in a buffer containing 50 mM Tris (pH 7.9), 300 mM NaCl, 1 mM dithiothreitol and 50% (v/v) glycerol at -20 °C. The protein concentrations were quantified by absorbance at 280 nm. Compounds N-306711, N-103019 and N-65828 were obtained from the National Cancer Institute. C-473872 and C-467929 were purchased from ChemBridge Corp. Benzopurpurin B and Congo red were purchased from Sigma-Aldrich (St. Louis, MO).

Molecular Modeling

The molecular docking program Dock 6.0 was used to execute flexible docking of the energy minimized inhibitor into the wild type sNsp15 crystal structure (PDB ID 2H85, (61)), which was kept rigid. A set of spheres that represent the negative image of the binding pocket was defined within the 10-Å radius of the sNSP15 catalytic-site residues H249, H234, K289, and Y342 to adopt the sphere-matching algorithm; incremental construction (anchor-and-grow method) was used to allocate the flexible conformations for the ligand. The automatic matching mode was used with 20 configurations per ligand building cycle. Interaction between the ligand and the receptor

was evaluated by the grid score (a combination of van der Waals and electrostatic components) followed by visual inspection.

Whether the inhibitor candidate could bind the MHV Nsp15 protein crystal structure (PDB ID 2GTH, (62)) over sNsp15 was analyzed by superimposing the latter docked with Benzopurpurin B over the former; for IBV a homology model was generated using Swiss-Model server (http://swissmodel.expasy.-org/SWISSMODEL.html) and superimposed on sNsp15 docked with Benzopurpurin B. The figures were prepared using UCSF Chimera (http://www.cgl.ucsf.edu/chimera/).

Endoribonuclease Assays

A real time endoribonuclease assay was performed as previously described (55). The assay used a substrate named rU from Integrated DNA Technologies, Inc. (Coralville, Iowa) whose fluorescence is quenched until cleavage at the uridylate. Fluorescence was monitored in a Fluorostar Optima (BMG Inc.) at excitation and emission wavelengths of 492 and 518 nm, respectively.

A gel-based RNA cleavage assay is used to confirm endoribonuclease activity and was performed as described previously (47). The 16-nt oligoribonucleotide substrate (GAAGCGAAACCCUAAG; Dharmacon Inc.) was labeled at the 5' end with [γ-^{32}P]-ATP and T4 polynucleotide kinase. Each reaction contained 10,000 cpm radiolabeled RNA substrate at a final concentration of 1 μM and 26 nM Nsp15 in Buffer T (50 mM Tris-HCl [pH 7.5], 50 mM KCl, 1 mM dithiothreitol and 5 mM $MnCl_2$). The reactions were incubated at 30 °C for 30 min and terminated by adding the gel-loading buffer

containing 90% (v/v) formamide. Products were separated by electrophoresis in 7.5 M urea, 20% (w/v) polyacrylamide gels. Gels were wrapped in plastic, and radiolabeled bands were quantified using a PhosphorImager (Molecular Dynamics).

Differential Scanning Fluorimetry

Differential scanning fluorimetry was performed in an Eppendorf Mastercycler EP realplex machine. Each sample was prepared in a total volume of 50 µL containing solutions of SARS-CoV Nsp15 at 2.5 µM final concentration, SYPRO orange (Molecular probes) at 2.5 X final concentration, and inhibitor in buffer T (100 mM Tris [pH 7.0], 50 mM KCl and 5 mM $MnCl_2$). The 96-well plate containing all of the samples was heated at a rate of 1.0 °C/min, from 25 to 95 °C, and the fluorescence intensity was measured with Ex/Em wavelengths of 470/550 nm. The Tm values were calculated by obtaining the maximum of the first derivative using Kaleidagraph (71). Each sample was tested in triplicate, and the results were duplicated in at least two independent assays.

Plaque Formation Assays

Mouse L2 cells were grown in DMEM with 10% serum medium in 6-well cell culture plates at 37 °C and 3% CO_2 for 48 h or until 100% confluent. MHV A59 dilutions (10^{-1} to 10^{-6}) were prepared in DMEM without serum. Virus inoculum and inhibitor were incubated 15 min at 4 °C. Cells were infected and incubated 1 h at room temperature then covered with 3 mL of a mixture 1:1 of 2X DMEM 2% serum and 1.6

% agarose (equilibrated to 45 °C). Plates were incubated at 37 °C and 3% CO_2 for 48 h, stained with a 1% crystal violet solution and the number of plaques formed was used to calculate the pfu/mL. Each inhibitor was tested at 100 μM in triplicate.

Labeling of Viral RNAs

L2 cells (2.25 x 10^5 per well) were seeded in 12-well plates and incubated at 37 °C in CO_2 incubator for 12 h. Cells were infected with MHV A59 at an MOI of 1 in the presence or absence of 100 μM inhibitor and further incubated for 6 h, washed twice with phosphate-free DMEM, fed with DMEM supplemented with 2 % dialyzed fetal bovine serum and actinomycin D (10 μg/ml) and incubated at 37 °C in CO_2 incubator. After a 15-min. incubation, the medium was replaced with phosphate-free DMEM supplemented with 2% dialyzed serum, 10 μg/ml actinomycin D and 200 μCi/ml $^{32}PO_4$. Cultures were further incubated at 37 °C in CO_2 incubator for 5.5 h. The radiolabeled cultures were washed twice with ice-cold phosphate-buffered saline and RNA was extracted using an RNeasy mini kit (Qiagen). Purified RNA was mixed with formaldehyde gel-loading buffer containing ethidium bromide, incubated at 65 °C for 15 min, chilled on ice and loaded onto a 1% formaldehyde-agarose gel. Electrophoresis was carried out at 100 V for 6 h. Following electrophoresis, the gel was illuminated with UV light and the image was captured with a BioDoc-It imaging system, and the relative amounts of 28S rRNA bands were determined by densitometry. The gel was then fixed

with 70 % methanol for 30 min, dried over vacuum and exposed to a PhosphorImager screen for quantification using Molecular Dynamics software.

RESULTS

Computational Docking of RNase A and Angiogenin Inhibitors

Compounds active against Ribonuclease A (70) and against Angiogenin (69), which have an Ribonuclease A active site, were selected for analysis against the SARS-CoV Nsp15 protein. The structures of the compounds are shown in Fig. 5A and B. We first formed a collaboration with Dr. S. Palanitathan of the Sacchettini laboratory to perform computational docking of the compounds into the structure of sNsp15 (PDB 2H85). The goal of this study was to determine whether the compounds are sterically and electronically compatible with the active site structure of sNsp15. The results in this section are from Dr. S. Palanitathan.

Small-molecule compounds N-65828, its analog Benzopurpurin B as well as two analogs of the compound C-181431, C-473872 and C-467929, and the compounds N-306711 and N-103019 were all predicted to bind to the enzyme active site by computational docking (Fig. 5C and 1D). All these inhibitors are predicted to interact with the active site groove formed by the residues Y342, H234, H249 and K289 and two cavities at either side of the active site. The docking scores were better for the Ribonuclease A inhibitors (Benzopurpurin B, C-473872, and C-467929) than for the Angiogenin inhibitors (Fig. 5E). In fact, the RNase A inhibitors were predicted to fully utilize the active site and the associated cavities present on either side of it. These results prompted us to also analyze the docking of Congo red, which is chemically similar to Benzopurpurin B except that it lacks the two methyl groups in the inner two

six-member rings, and this is expected to alter the conformation of the compound. Congo red had a slightly better docking score (-57.78) than Benzopurpurin B and was thus added to the compounds that we would test in functional assays.

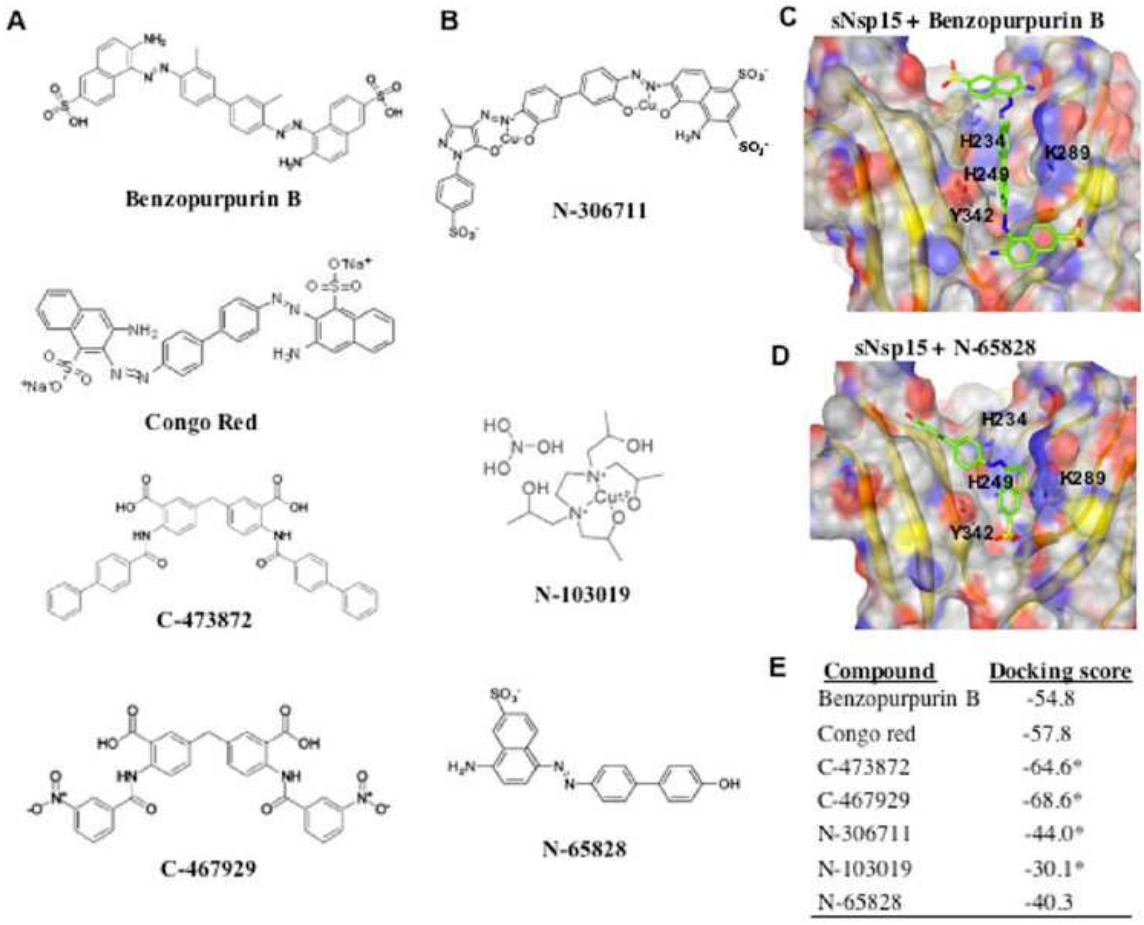

FIGURE 5. **Small molecule inhibitors tested for effects on Nsp15.** A, inhibitors of Ribonuclease A previously reported by Jenkins *et al.* (70). Congo red, a Benzopurpurin B analog was also assayed. B, inhibitors of Angiogenin previously reported by Kao *et al*. (69). C, the docking of Benzopurpurin B to the catalytic site of SARS-CoV Nsp15. The docking conformation with the higher score is shown. The C-terminal active site groove is shown in a yellow ribbon representation under a semi-transparent surface colored by atom. The catalytic site residues are labeled. The inhibitor stacks with Y342 residue and occupies the entire C-terminal active site groove of sNsp15. D, the docking conformation of N-65828 in the sNsp15 catalytic site. E, docking scores of the inhibitors tested. Panels C, D and E by Palaninathan S.

Effects of the Inhibitors on sNsp15 Endoribonuclease Activity

A real-time fluorescence assay and highly purified recombinant sNsp15 protein were used to examine the efficacy of the inhibitors against sNsp15 *in vitro* (55). All of the compounds showed a concentration-dependent inhibition of sNsp15 endoribonuclease activity and an examination of the output of such an assay performed with Benzopurpurin B is shown in Fig. 6A.

To confirm that the real time cleavage results are illustrative of an inhibition of RNA cleavage activity, the effects of the compounds on the cleavage of a previously characterized 16-nt RNA in a gel-based assay was performed. The results were found to be consistent with those from the real time assay (Fig. 6B). The remainder of the results presented will be from the real time assay.

The concentration of inhibitors needed to reduce sNsp15 endoribonuclease activity by 50 and 90% (IC_{50} and IC_{90}, respectively), were determined for each of the compounds used in the molecular docking reaction. Inhibitor titration experiments with Benzopurpurin B and Congo red are shown in Fig. 6C and a summary of all of the IC_{50} and IC_{90}s are shown in Fig. 6D. Of all the compounds tested, Benzopurpurin B was the best inhibitor, with IC_{50} and IC_{90} of 0.2 and 0.9 μM, respectively. We also note that while functional examination of the effects of the inhibitors on endoribonuclease activities confirmed that the Ribonuclease A inhibitors were more effective than the Angiogenin inhibitors, the relative ranking of the results from two assays did not correspond.

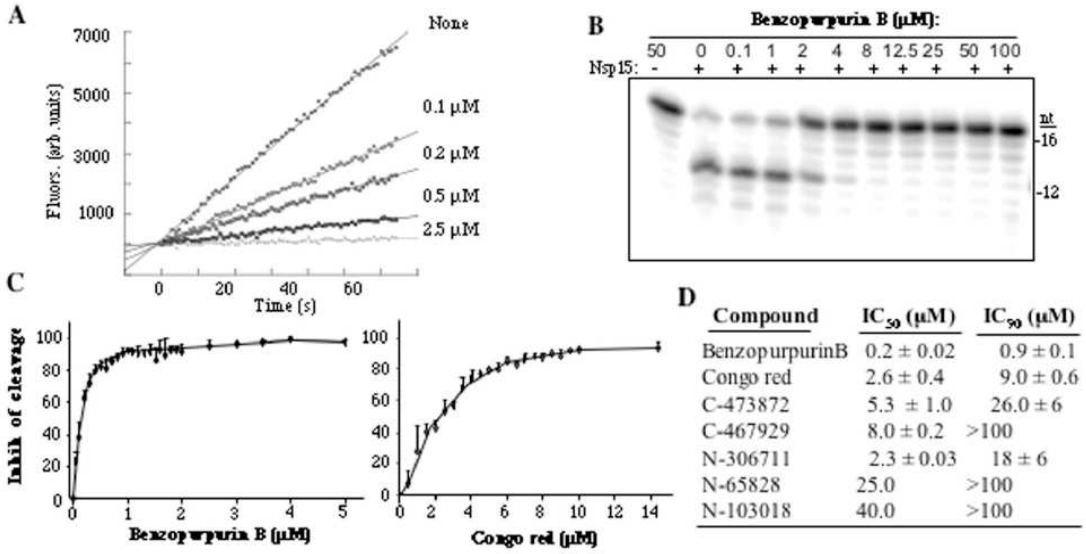

FIGURE 6. **Effects of the small molecule inhibitors on the SARS-CoV Nsp15 endoribonuclease activity.** A, representative results of a real-time endoribonuclease assay showing the inhibitory effect of Benzopurpurin B at different concentrations on the sNsp15 activity. The slope of the change in fluorescence was used to determine the rate of cleavage by Nsp15. B, a demonstration of the results from a gel-based RNA cleavage assay in presence of increasing concentrations of Benzopurpurin B. C, Benzopurpurin B and Congo red titrations plots using the real-time endoribonuclease assay. Concentration dependent inhibition of the substrate cleavage by sNsp15 is shown. D, summary of the IC50 and IC90 values for the small molecule compounds tested.

Mechanism of Action of Select Inhibitors

To demonstrate that the compounds could bind to the sNsp15, we tested for changes in Nsp15 in response to temperature. The assays were performed using differential scanning fluorimetry in the presence of the dye SYPRO Orange, which binds to the hydrophobic regions of a protein that are exposed by temperature-induced unfolding. The transition curves are complex, as would be expected by the unfolding of an oligomeric protein, however, a major peak could be readily identified (Fig. 7A). The temperature where there is a maximal transition in this peak will be designated the

Tm_{app}. All samples were tested in triplicate and in a buffer capable of supporting enzymatic activity that included 5 mM Mn^{2+}, which we observed to help in smoothing the changes in transition, likely by affecting sNsp15 conformation, as previously demonstrated by Bhardwaj *et al.* (2004), (47). The sNsp15 protein had a Tm_{app} at 49 ^{o}C in the absence of ligand. In the presence of Benzopurpurin B at 1, 3 and 5 μM final concentration, the Tm_{app} values were 49, 55 and 56°C respectively (Fig. 7B). A reaction performed in the absence of sNsp15, but in the presence of these concentrations of Benzopurpurin B or other inhibitors tested did not change the fluorescence of SYPRO orange. The change in the Tm_{app} provides evidence for the interaction between the compounds and sNsp15. Compound C-473872 at 5, 10 and 20 μM also increased the Tm_{app} values in a concentration-dependent manner (Fig. 7B). Unexpectedly, while Congo red did cause a concentration-dependent change, there was decrease in the $Tm_{app.}$

Given that the inhibitors were originally active site inhibitors of Ribonuclease A and Angiogenin, it is likely that they will act as competitive inhibitors of sNsp15. The inhibitory effects of Benzopurpurin B, Congo red, and C-473872 were tested at several concentrations, and the results from a minimum of three independent analyses were averaged and analyzed by a double reciprocal plot. The results are compatible with inhibition of SARS-CoV Nsp15 by a competitive mechanism (Fig. 7C). According to this mechanism the compounds are able to bind to the free enzyme active site, competing with the substrate. Because not all of the plots crossed at the zero in the axes, these results do not rule out the presence of additional ligand binding sites or that all of the active sites bind to the inhibitors in the same manner. In fact, crystal structure of the

Nsp15 revealed that there is a significant difference in the active sites of the six subunits of Nsp15 and that the difference is particularly distinct between the two trimers of Nsp15.

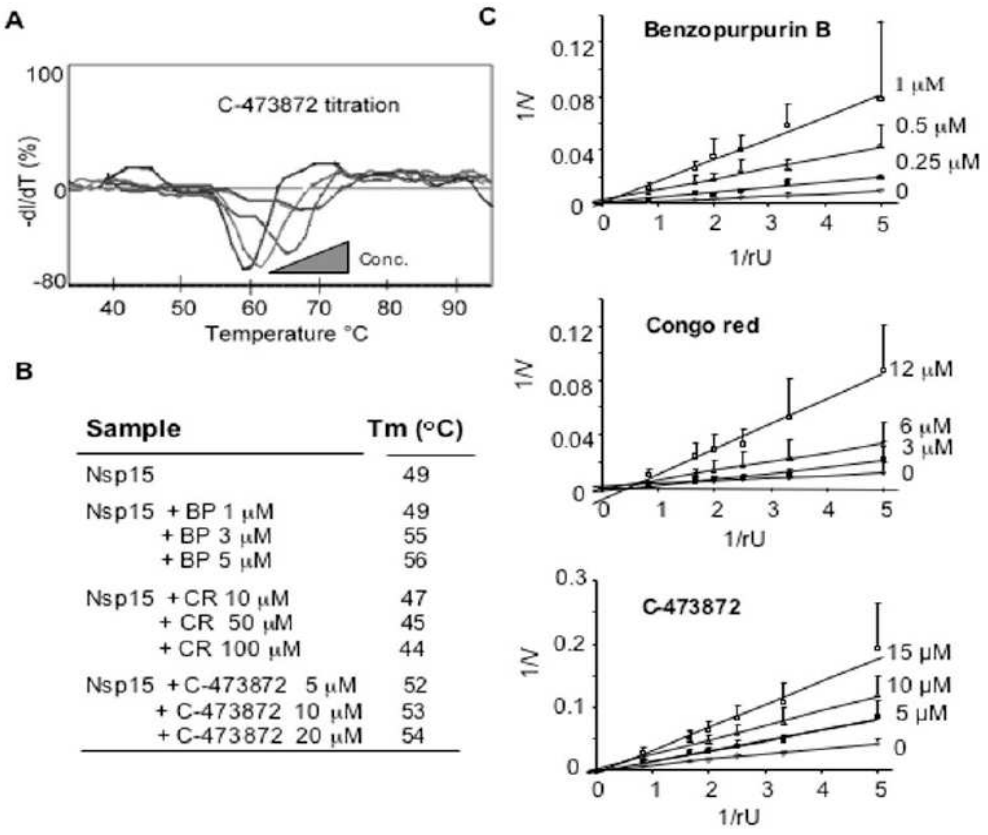

Sample	Tm (°C)
Nsp15	49
Nsp15 + BP 1 μM	49
+ BP 3 μM	55
+ BP 5 μM	56
Nsp15 + CR 10 μM	47
+ CR 50 μM	45
+ CR 100 μM	44
Nsp15 + C-473872 5 μM	52
+ C-473872 10 μM	53
+ C-473872 20 μM	54

FIGURE 7. **Mechanism of inhibition of Nsp15 by select inhibitors.** A, first derivative of the differential scanning fluorimetry assays for C-473872. A peak for each curve is obtained at the Tm. A shift of the Tm values corresponding to each peak is observed in the presence of increasing concentrations of compound. B, summary of the Tm data obtained by differential scanning fluorimetry in the presence of Benzopurpurin B (BP), Congo red (CR) and C-473872. A shift in the Tm values is indicative of binding to the compound to sNsp15. C, double reciprocal plot analysis for Benzopurpurin B, Congo red and C-473872. A change in the slope of the plots upon increasing inhibitor concentrations is characteristic of a competitive mechanism of inhibition.

The MHV and IBV Nsp15 Activity are Inhibited by Benzopurpurin B *in vitro*

Coronaviruses can be important pathogens of animals as well as humans (9, 10, 11). Elucidation of the structure of the MHV Nsp15 (mNsp15) and molecular modeling revealed that the active site structure is highly similar to that of the SARS-CoV Nsp15 (62, 64, Fig. 8A). We wanted to determine whether an inhibitor active against the SARS-CoV Nsp15 will have similar effects on the Nsp15 proteins of other coronaviruses. Superimposition of sNsp15 docked with Benzopurpurin B on top of mNsp15 showed that Benzopurpurin-like inhibitors could be accommodated within the MHV Nsp15 active site (Fig. 8A); the flexibility of the C-terminal active site can further augment the binding. When tested for effects on RNA cleavage by the MHV Nsp15 protein expressed in *E. coli*, Benzopurpurin B was found to have an IC_{50} and IC_{90} of 0.4 and 0.9 μM, highly similar to the values obtained with the SARS-CoV Nsp15 (Fig. 8B).

To extend the analysis further, we tested the effects of Benzopurpurin B on the Nsp15 ortholog of infectious bronchitis virus (IBV), iNsp15, which was demonstrated by Bhardwaj *et al.* (2004) (47) to specifically cleave uridylates. Since the iNsp15 structure has not been determined, we threaded its sequence into the crystal structure of the SARS-CoV. The active site of the protein was essentially comparable to that of the SARS-CoV and MHV orthologs and could accommodate Benzopurpurin B (Fig. 8C). A prediction of this analysis is that the iNsp15 will also be inhibited by the compounds effective on the MHV and SARS-CoV Nsp15. Indeed, the iNsp15 was inhibited by Benzopurpurin B in a concentration-dependent manner and with IC_{50} and IC_{90} values similar to that of the MHV and SARS-CoV Nsp15 enzymes (Fig. 8D). These results

suggest that the Nsp15 orthologs from these three coronaviruses likely have highly similar active site pockets. Furthermore, it should be possible to use model coronaviruses to study the effects of these drugs on viral infection under conditions that do not require BSL3 containment.

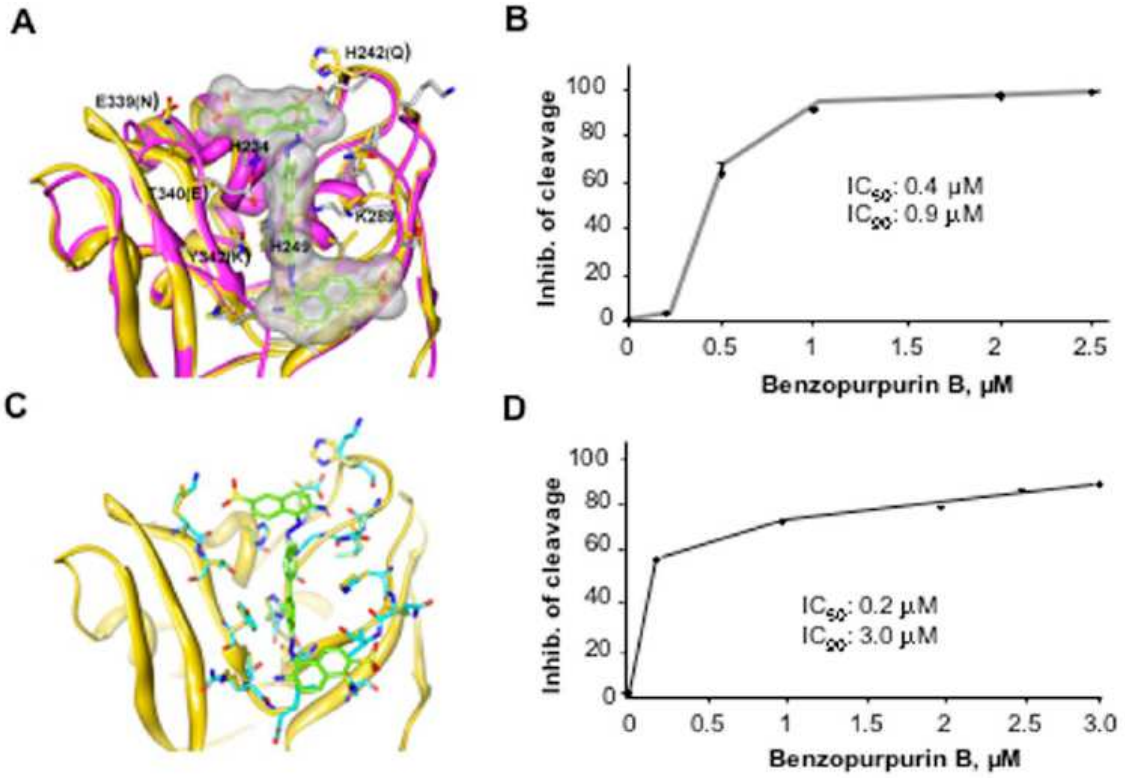

FIGURE 8. **Inhibition of RNA cleavage *in vitro* in other coronavirus Nsp15 orthologs.** A, a model for the binding of Benzopurpurin B in the MHV Nsp15 crystal structure (magenta ribbon and grey sticks; PDB ID 2gth). Althought the catalytic site residues are identical, the nearby residues are not conserved between sNsp15 and mNsp15, non-conserved residues are shown in parenthesis. Perhaps the flexibility of the C-terminal active site residues should enable the inhibitor binding to mNsp15 as well. B, effects of Benzopurpurin B on the MHV Nsp15 ortholog. The enzyme is inhibited in a concentration dependent manner. C, a model of the IBV Nsp15 ortholog. The active site residues in the IBV Nsp15 homology model are well conserved with the SARS-CoV Nsp15. D, Effects of benzopurpurin B on endoribonuclease activity of the IBV Nsp15 ortholog using the real-time fluorescence assay.

Inhibition of MHV Infection in Cultured Cells

The effect of the compounds on MHV replication was investigated in plaque formation assays using mouse L2 cells. The cells were plated in six-well cell culture plates and grown until 100% confluence then infected with different dilutions of MHV A59 and the inhibitor at a final concentration of 100 μM. After a 1 h period to allow the infection to initiate, the cells were covered with a mixture of medium and agarose and incubated for two days, when the plaques were stained and scored. In three independent experiments, Congo red reproducibly showed the most inhibition of MHV plaque formation, with the mean reduction of plaque formation being 26-fold. Compound C-473872 caused an 11-fold reduction, and Benzopurpurin B, despite being the best inhibitor *in vitro*, resulted in an 8-fold reduction. None of the compounds had any obvious effect on the shape or viability of the cells when present at 100 μM (Fig. 9A, 9B and data not shown).

To confirm and extend the analysis of the compounds on MHV infection, Dr. Kanchan Bhardwaj examined MHV RNA production in the presence of Benzopurpurin B, Congo red and C-473872. Genomic and subgenomic RNAs were reduced in the presence of the drugs, with C-473872 being the most effective and Benzopurpurin B having only a minimal effect in cells. Furthermore, both the genomic and subgenomic MHV RNA levels were uniformly affected (Fig. 9C).

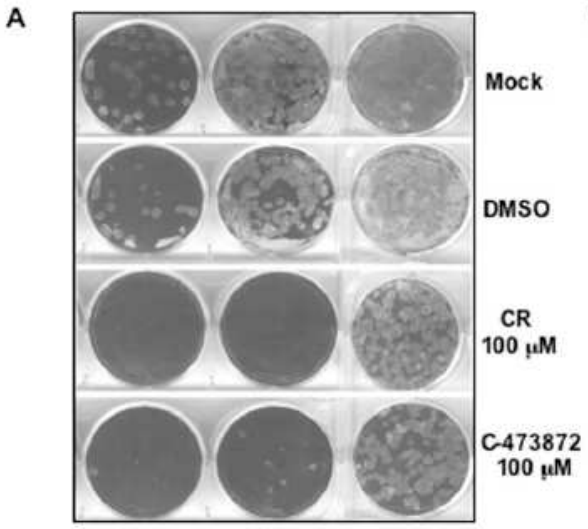

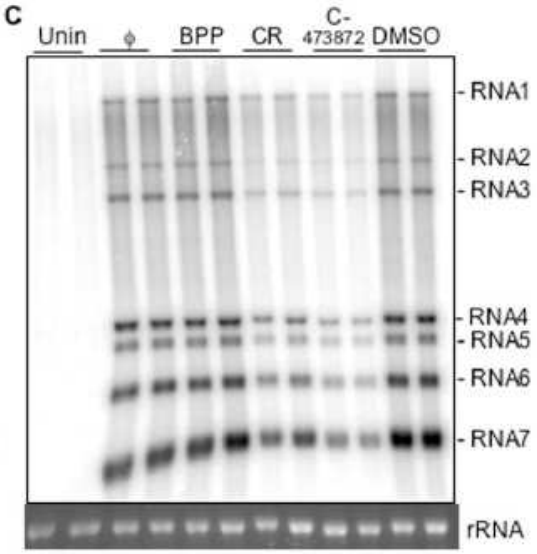

B

Compound, conc.	Pfu/mL	Fold reduc. (N=3)
Mock	1.8×10^7	
Benzopurpurin B, 100 μM	2.2×10^6	**8.0 ± 0.2**
Congo Red, 100 μM	6.6×10^5	**26.0 ± 0.3**
Mock	4.9×10^6	
C-473872, 100 μM	4.9×10^5	**11.0 ± 2**
C-467929, 100 μM	3.0×10^6	**1.3 ± 3**
N-306711, 100 μM	8.5×10^6	**1.3 ± 0.1**

FIGURE 9. **Effects of select Nsp15 inhibitors on MHV plaque formation in mouse L2 cells.** A, representative plaque assay results in presence of Congo red and C-473872 at 100 uM, or controls such as the solvent DMSO. B, summary of the effects of the small-molecule compounds on MHV replication in L2 cells. The number of PFU/mL obtained and the fold reduction observed in three independent assays are reported. C, effects of the compounds on MHV RNA accumulation. The identities of the RNAs are shown to the left of the gel image. The rRNAs are intended to serve as a loading control. The result in panel C was obtained by Bhardwaj K.

DISCUSSION

The development of both vaccines and anti-virals specific against coronavirus infections is currently a need. The Nsp15 endoribonuclease is a genetic marker for coronaviruses and is an unusual enzyme for RNA viruses. Based on the observation that Nsp15 has an Ribonuclease A-like active site and a mechanism for RNA cleavage identical to Ribonuclease A (61, 64) we tested previously identified inhibitors of Ribonuclease A and Angiogenin, a Ribonuclease A-like enzyme.

Computational docking into the structure of sNsp15 predicted that small-molecule inhibitors of Angiogenin and RNase A could bind to the Nsp15 active site. Functionally, three Angiogenin and RNase A inhibitors, C-473872, C-467929, Benzopurpurin B, and the structurally related Congo red, were found to be potent inhibitors of the sNsp15 endoribonuclease activity *in vitro*. To put this into context, more than 50 candidates with high probability of docking into the sNsp15 active site were tested previously and no compounds were found to have IC_{50} values better than 50 μM (Bhardwaj et al. unpublished data). Surprisingly, four inhibitors out of seven with IC_{50}s of better than 10 μM were found. The results add a layer of functional relevance to the claims that sNsp15 has an RNase A-like catalytic pocket and cleavage mechanism for the Nsp15 of different coronaviruses (61, 64).

Benzopurpurin B, Congo red, and C-473872 were able to bind sNsp15 since they induce a concentration-dependent shift of the T_m of sNsp15. Benzopurpurin B and C-473872 induce an increase in the sNsp15 Tm that corresponds to a stabilizing effect of

the compounds. Interestingly, Congo red induces the T_m to decrease, suggesting that it destabilized the protein. Since Benzopurpurin B and C-473872 are active site inhibitors of RNase A and Angiogenin (69, 70), and Congo red is likely to be one as well, and the three compounds could bind to the sNsp15 active site according to computational docking models, it is logical to assume that these compounds are competitive inhibitors. The inhibition curves suggest this as well. However, at the present time, we cannot rule out the presence of additional binding sites for these compounds in sNsp15.

Benzopurpurin B showed to inhibit the MHV and IBV Nsp15 orthologs similarly to sNsp15, suggesting that the Nsp15 orthologs from these three coronaviruses likely have highly similar active site pockets, which supports previous structural and mutational studies of the mNsp15 (59, 62).

Importantly, Congo red and C-473872 reduced the infection of MHV in cultured cells by several fold. The structures of these compounds should be considered as leads for subsequent development of coronavirus inhibitors. The best inhibitor in biochemical assays, Benzopurpurin B, was not particularly effective in virus-infected cells. This is likely due to pharmacological properties of Benzopurpurin B, like half-life in solution or in the cells or the ability to enter cells, features that we have not pursued in this work. Notably, the fact that Benzopurpurin B differed from Congo red only by the presence of two methyl groups indicates that small modifications to Congo red or Benzopurpurin B could have dramatic effects on the efficacy of these compounds in cells.

Congo red is also a promising lead compound in the imaging and treatment of amyloid protein plaques (72, 73). Its ability to interact with nucleotide-binding enzymes

explains in part its efficacy to inhibit RNase A and Nsp15 (74). Congo red and its derivatives when administered near the time of infection have been shown to delay the onset of clinical disease in scrapie infected hamsters (75). However, Congo red is potentially toxic due to its degradation into the carcinogenic compound benzidine and several derivatives have been tested for anti-amyloid properties (76). These compounds would be of interest for testing its efficacy to treat coronavirus infections.

The compounds can also serve as new tools to analyze coronavirus infection. A proposed role for Nsp15 is that it may participate in the processing of the RNAs needed to form coronavirus subgenomic RNAs (8). However, there is no direct evidence for this in MHV. The compounds induced a reduction in the MHV RNA levels affecting uniformly genomic and subgenomic RNAs. In fact, mutational analysis of the mNsp15 resulted in a general decrease in all MHV RNAs and an approximately one log decrease in MHV virion production. If Nsp15 does have a direct effect on subgenomic RNA production, the effects are sufficiently pleiotropic to affect all MHV RNAs (59). The effects of the inhibitors on MHV RNA production are consistent with those from previous mutational analyses (59). More judicious application of Congo red and C-473872 at different stages of coronavirus infection in cultured cells could allow better insight into how Nsp15 contributes to this process.

CONCLUSIONS

The Nsp15 endoribonuclease is a genetic marker for coronaviruses and is an unusual enzyme for RNA viruses which makes it a promising target for new antiviral therapies.

Nsp15 active site and mechanism similarities to Ribonuclease A (61, 64) led us to test previously identified inhibitors of Ribonuclease A and Angiogenin, a Ribonuclease A-like enzyme.

Computational docking into the structure of sNsp15 predicted that small-molecule inhibitors of Angiogenin and RNase A could bind to the Nsp15 active site. Three Angiogenin and RNase A inhibitors, C-473872, C-467929, Benzopurpurin B, and the structurally related Congo red, were found to be potent inhibitors of the sNsp15 endoribonuclease activity *in vitro* with IC_{50} of less than 10 μM.

Benzopurpurin B, Congo red, and C-473872 were able to bind sNsp15 since they induce a concentration-dependent shift of the T_m of sNsp15. As predicted by the docking models they are active site inhibitors of sNsp15 according to double reciprocal analysis.

Benzopurpurin B inhibited the MHV and IBV Nsp15 orthologs similarly to sNsp15, suggesting that the Nsp15 orthologs from these three coronaviruses likely have highly similar active site pockets, which supports previous structural and mutational studies of the mNsp15.

Congo red and C-473872 reduced the infection of MHV in cultured cells by several fold. The structures of these compounds should be considered as leads for subsequent development of coronavirus inhibitors.

The compounds induced a reduction in the MHV RNA levels affecting uniformly genomic and subgenomic RNas.

The compounds can also serve as new tools to analyze coronavirus infection.

REFERENCES

1. Peiris, J. S., Yuen, K. Y., Osterhaus, A. D., and Stohr, K. (2003) *N. Engl. J. Med.* **349,** 2431-2441

2. Poutanen, S. M., Low, D. E., Henry, B., Finkelstein, S., Rose, D., Green, K., Tellier, R., Draker, R., Adachi, D., Ayers, M., Chan, A. K., Skowronski, D.M., Salit, I., Simor, A. E., Slutsky, A. S., Doyle, P. W., Krajden, M., Petric, M., Brunham, R. C., and McGeer, A. J. (2004) *N. Engl. J. Med.* **348,** 1995-2005

3. Christian, M. D., Poutanen, S. M., Loutfy, M. R., Muller, M. P., and Low, D. E. (2004) *Clin. Infect. Dis.* **38,** 1420-1427

4. Guan, Y., Zheng, B. J., He, Y. Q., Liu, X. L., Zhuang, Z. X., Cheung, C. L., Luo, S. W., Li, P. H., Zhang, L. J., Guan, Y. J., Butt, K. M., Wong, K. L., Chan, K.W., Lim, W., Shortridge, K. F., Yuen, K. Y., Peiris, J. S., and Poon, L. L. (2003) *Science* **302,** 276-278

5. Song, H. D., Tu, C. C., Zhang, G. W., Wang, S. Y., Zheng, K., Lei, L. C., Chen, Q. X., Gao, Y. W., Zhou, H. Q., Xiang, H., Zheng, H. J., Chern, S. W., Cheng, F., Pan, C. M., Xuan, H., Chen, S. J., Luo, H. M., Zhou, D. H., Liu, Y. F., He, J. F., Qin, P. Z., Li, L. H., Ren, Y. Q., Liang, W. J., Yu, Y. D., Anderson, L., Wang, M., Xu, R. H., Wu, X. W., Zheng, H. Y., Chen, J. D., Liang, G., Gao, Y., Liao, M., Fang, L., Jiang, L. Y., Li, H., Chen, F., Di, B., He, L. J., Lin, J. Y., Tong, S., Kong, X., Du, L., Hao, P., Tang, H., Bernini, A., Yu, X. J., Spiga, O., Guo, Z. M., Pan, H. Y., He, W. Z., Manuguerra, J. C., Fontanet, A., Danchin, A., Niccolai, N., Li, Y. X., Wu, C. I., and Zhao, G. P. (2005) *Proc. Natl. Acad. Sci. U. S. A.* **102,** 2430-2435

6. Li, W., Shi, Z., Yu, M., Ren, W., Smith, C., Epstein, J. H., Wang, H., Crameri, G., Hu, Z., Zhang, H., Zhang, J., McEachern, J., Field, H., Daszak, P., Eaton, B. T., Zhang, S., and Wang, L. F. (2005) *Science* **310,** 670-679

7. Cheng, V. C., Lau, S. K., Woo, P. C., and Yuen, K. Y. (2007) *Clin. Microbiol. Rev.* **20,** 660-694

8. Snijder, E. J., Bredenbeek, P. J., Dobbe, J. C., Thiel, V., Ziebuhr, J., Poon, L. L., Guan, Y., Rozanov, M., Spaan, W. J., and Gorbalenya, A. E. (2003) *J. Mol. Biol.* **331,** 991-1004

9. Masters, P. S. (2006) *Adv. Virus Res.* **66,** 193-292

10. Lai, M. M., and Cavanagh, D. (1997) *Adv. Virus Res.* **48,** 1-100

11. Spaan, W., Cavanagh, D., and Horzinek, M. C. (1988) *J. Gen. Virol*. **69,** 2939-2952

12. Gorbalenya, A. E., Snijder, E. J., and Spaan, W. J. (2004) *J. Virol.* **78,** 7863-7866

13. Lau, S. K., Woo, P. C., Li, K. S., Huang, Y., Tsoi, H. W., Wong, B. H., Wong, S. S., Leung, S. Y., Chan, K. H., and Yuen, K. Y. (2005) *Proc. Natl. Acad. Sci. U. S. A.* **102,** 14040-14045

14. McIntosh, K. (1974) *Curr. Top. Microbiol. Imunol*. **63,** 85-129

15. Macnaughton, M. R., Davies, H. A., and Nermut, M. V. (1978) *J. Gen. Virol*. **39,** 545-549

16. Marra, M. A., Jones, S. J., Astell, C. R., Holt, R. A., Brooks-Wilson, A., Butterfield, Y. S., Khattra, J., Asano, J. K., Barber, S. A., Chan, S. Y., Cloutier, A., Coughlin, S. M., Freeman, D., Girn, N., Griffith, O. L., Leach, S. R., Mayo, M., McDonald, H., Montgomery, S. B., Pandoh, P. K., Petrescu, A. S., Robertson, A. G., Schein, J. E., Siddiqui, A., Smailus, D. E., Stott, J. M., Yang, G. S., Plummer, F., Andonov, A., Artsob, H., Bastien, N., Bernard, K., Booth, T. F., Bowness, D., Czub, M., Drebot, M., Fernando, L., Flick, R., Garbutt, M., Gray, M., Grolla, A., Jones, S., Feldmann, H., Meyers, A., Kabani, A., Li, Y., Normand, S., Stroher, U., Tipples, G. A., Tyler, S., Vogrig, R., Ward, D., Watson, B., Brunham, R. C., Krajden, M., Petric, M., Skowronski, D. M., Upton, C., and Roper, R. L. (2003) *Science* **300,** 1399-1404

17. Rota, P. A., Oberste, M. S., Monroe, S. S., Nix, W. A., Campagnoli, R., Icenogle, J. P., Penaranda, S., Bankamp, B., Maher, K., Chen, M. H., Tong, S., Tamin, A., Lowe, L., Frace, M., DeRisi, J. L., Chen, Q., Wang, D., Erdman, D. D., Peret, T. C., Burns, C., Ksiazek, T. G., Rollin, P. E., Sanchez, A., Liffick, S., Holloway, B., Limor, J., McCaustland, K., Olsen-Rasmussen, M., Fouchier, R., Gunther, S., Osterhaus, A. D., Drosten, C., Pallansch, M. A., Anderson, L. J., and Bellini, W. J. (2003) *Science* **300,** 1394-1399

18. Thiel, V., Ivanov, K. A., Putics, A., Hertzig, T., Schelle, B., Bayer, S., Weissbrich, B., Snijder, E. J., Rabenau, H., Doerr, H. W., Gorbalenya, A. E., and Ziebuhr, J. (2003) *J. Gen. Virol*. **84,** 2305-2315

19. Wong, S. K., Li, W., Moore, M. J., Choe, H., and Farzan, M. (2004) *J. Biol. Chem*. **279,** 3197-3201

20. Sui, J., Li, W., Murakami, A., Tamin, A., Matthews, L. J., Wong, S. K., Moore, M. J., Tallarico, A. S., Olurinde, M., Choe, H., Anderson, L. J., Bellini, W. J.,

Farzan, M., and Marasco, W. A. (2004) *Proc. Natl. Acad. Sci. U. S. A.* **101,** 2536-2541

21. Yeager, C. L., Ashmun, R. A., Williams, R. K., Cardellichio, C. B., Shapiro, L. H., Look, A. T., and Holmes, K. V. (1992) *Nature* **357,** 420-422

22. Williams, R. K., Jiang, G. S., and Holmes, K. V. (1991) *Proc. Natl. Acad. Sci. U. S. A*. **88,** 5533-5536

23. Li, W., Moore, M. J., Vasilieva, N., Sui, J., Wong, S. K., Berne, M. A., Somasundaran, M., Sullivan, J. L., Luzuriaga, K., Greenough, T. C., Choe, H., and Farzan, M. (2003) *Nature* **426,** 450-454

24. Hamming, I., Timens, W., Bulthuis, M. L., Lely, A. T., Navis, G. J., and van Goor, H. (2004) *J.Pathol*. **203,** 631-637

25. Liu, S., Xiao, G., Chen, Y., He, Y., Niu, J., Escalante, C. R., Xiong, H., Farmar, J., Debnath, A. K., Tien, P., and Jiang, S. (2004) *Lancet* **363,** 938-947

26. Bosch, B. J., Martina, B. E., Van Der Zee, R., Lepault, J., Haijema, B. J., Versluis, C., Heck, A. J., De Groot, R., Osterhaus, A. D., and Rottier, P. J. (2004) *Proc. Natl. Acad. Sci. U. S. A.* **101,** 8455-8460

27. Herold, J., Siddell, S. G., and Gorbanleya, A. E. (1999) *J. Biol. Chem*. **274,** 14918-14925

28. Tijms, M. A., van Dinten, F. C., Gorbanleya, A. E., and Snijder, E. J. (2001) *Proc. Natl. Acad. Sci. U. S. A.* **98,** 1889-1894

29. Ziebuhr, J. (2005) *Curr. Top. Microbiol. Immunol*. **287,** 57-94

30. Ziebuhr, J., Snijder, E. J., and Gorbalenya, A. E. (2000) *J. Gen. Virol*. **81,** 853-879

31. Ziebuhr, J. (2004) *Curr. Opin. Microbiol*. **7,** 412-419

32. Jacobs, L., Spaan, W. J. M., Horzinek M. C., and van der Zeijst, B. A. M. (1981) *J. Virol.* **39,** 401-406

33. Makino, S., Stohlman, S. A., and Lai, M. M. C. (1986) *Proc. Natl. Acad. Sci. U. S. A.* **83,** 4204-4208

34. Lai, M. M. C. (1986) *BioEssays* **5,** 257-260

35. Zuniga, S., Sola, I., Alonso, S., and Enjuanes, L. (2004) *J. Virol*. **78,** 980-994

36. Sawiki, S. G., and Sawiki, D. L. (1998) *Adv. Exp. Med. Biol*. **440,** 215-219

37. Sawiki, S. G., and Sawiki, D. L. (2005) *Curr. Top. Microbiol. Immunol.* **287,** 31-55

38. Sawiki, S. G., and Sawiki, D. L. (1990) *J. Virol.* **64,** 1050-1056

39. Sethna, P., Hofmann, M., and Brian, D. (1991) *J. Virol*. **65,** 320-325

40. Sethna, P., Hung, S., and Brian, D. (1989) *Proc. Natl. Acad. Sci. U. S. A.* **86,** 5626-5630

41. Pasternak, A. O., van der Born, E., Spaan, W. J. M., and Snijder, E. J. (2001) *EMBO J.* **20,** 7220-7228

42. Pasternak, A. O., van der Born, E., Spaan, W. J. M., and Snijder, E. J. (2003) *J. Virol.* **77,** 1175-1183

43. Pasternak, A. O., Spaan, W. J. M., and Snijder, E. J. (2003) *J. Virol.* **78,** 8102-8113

44. van Marle, G., Dobbe, J. C., Gultyaev, A. P., Luytjes, Spaan, W. J. M., and Snijder, E. J. (1999) *Proc. Natl. Acad. Sci. U. S. A.* **96,** 12056-12061

45. Imbert, I., Guillemot, J. C., Bourhis, J. M., Bussetta, C., Coutard, B., Egloff, M. P., Ferron, F., Gorbalenya, A. E., and Canard, B. (2006) *EMBO J.* **25,** 4933-4942

46. Minskaia, E., Hertzig, T., Gorbalenya, A. E., Campanacci, V., Cambillau, C., Canard, B., and Ziebuhr, J. (2006) *Proc. Natl. Acad. Sci. U. S. A.* **103,** 5108-5113

47. Bhardwaj, K., Guarino, L., and Kao, C. C. (2004) *J. Virol*. **78,** 12218-12224

48. Ivanov, K. A., Hertzig, T., Rozanov, M., Bayer, S., Thiel, V., Gorbalenya, A. E., and Ziebuhr, J. (2004) *Proc. Natl. Acad. Sci. U. S. A.* **101,** 12694-12699

49. Brockway, S. M., Clay, C. T., Lu, X. T., and Denison, M. R. (2003) *J. Virol*. **77,** 10515-10527

50. Cheng, A., Zhang, W., Xie, Y., Jiang, W., Arnold, E., Sarafianos, S. G., and Ding, J. (2005) *Virology* **335,** 165-176

51. Ivanov, K. A., Thiel, V., Dobbe, J. C., van der Meer, Y., Snijder, E. J., and Ziebuhr, J. (2004) *J. Virol*. **78,** 5619-5632

52. Ivanov, K. A., and Ziebuhr, J. (2004) *J. Virol*. **78,** 7833-7838

53. Tanner, J. A., Watt, R. M., Chai, Y. B., Lu, L. Y., Lin, M. C., Peiris, J. S., Poon, L. L., Kung, H. F., and Huang, J. D. (2003) *J. Biol. Chem*. **278,** 39578-39582

54. Seybert, A., Hegyi, A., Siddell, S. G., and Ziebuhr, J. (2000) *RNA* **6,** 1056-1068

55. Bhardwaj, K., Sun, J., Holzenburg, A., Guarino, L. A., and Kao, C. C. (2006) *J. Mol. Biol*. **361,** 243-256

56. Caffarelli, E., Maggi, L., Fatica, A., Jiricny, J., and Bozzoni, I. (1997) *Biochem. Biophys. Res. Commun.* **233,** 514-517

57. Laneve, P., Altieri, F., Fiori, M. E., Scaloni, A., Bozzoni, I., and Caffarelli, E. (2003) *J. Biol. Chem.* **278,** 13026-13032

58. Posthuma, C. C., Nedialkova, D. D., Zevenhoven-Dobbe, J. C., Blokhuis, J. H., Gorbalenya, A. E., and Snijder, E. J. (2006) *J. Virol.* **80,** 1653-1661

59. Kang, H., Bhardwaj, K., Li, Y., Palaninathan, S., Sacchettini, J., Guarino, L., Leibowitz, J. L., and Kao, C. C. (2007) *J. Virol.* **81,** 13587-13597

60. Guarino, L. A., Bhardwaj, K., Dong, W., Sun, J., Holzenburg, A., and Kao, C. (2005) *J. Mol. Biol*. **353,** 1106-1117

61. Ricagno, S., Egloff, M. P., Ulferts, R., Coutard, B., Nurizzo, D., Campanacci, V., Cambillau, C., Ziebuhr, J., and Canard, B. (2006) *Proc. Natl. Acad. Sci .U. S. A.* **103,** 11892-11897

62. Xu, X., Zhai, Y., Sun, F., Lou, Z., Su, D., Xu, Y., Zhang, R., Joachimiak, A., Zhang, X. C., Bartlam, M., and Rao, Z. (2006) *J.Virol*. **80,** 7909-7917

63. Roberts, G., Dennis, E. A., Meadows, D. H., Cohen, J. S., and Jardentzky, O. *Proc. Natl. Acad. Sci .U. S. A.* **62,** 1151-1158

64. Bhardwaj, K., Palaninathan, S., Alcantara, J. M., Yi, L. L., Guarino, L., Sacchettini, J. C., and Kao, C. C. (2008) *J. Biol. Chem*. **283,** 3655-3664

65. Saida, F., Uzan, M., and Bontems, F. (2003) *Nucleic Acids Res.* **31,** 2751-2758

66. Deshpande, R. A., and Shankar, V. (2002) *Crit. Rev. Microbiol*. **28,** 79-122

67. Gioia, U., Laneve, P., Dlakic, M., Arceci, M., Bozzoni, I., and Caffarelli, E. (2005) *J. Biol. Chem*. **280,** 18996-19002

68. Nowotny, M., Gaidamakov, S. A., Crouch,R.J., and Yang, W. (2005) *Cell* **121,** 1005-1016

69. Kao, R.Y., Jenkins, J. L., Olson, K. A., Key, M. E., Fett, J. W., and Shapiro, R. (2002) *Proc. Natl. Acad. Sci. U. S. A.* **99,** 10066-10071

70. Jenkins, J. L., and Shapiro, R. (2003) *Biochemistry* **42,** 6674-6687

71. Niesen, F. H., Berglund, H., and Vedadi, M. (2007) *Nature Protocols* **2,** 2212-2221

72. Furumoto, S., Okamura, N., Iwata, R., Yanai, K., Arai, H., and Kudo,Y. (2007) *Curr. Top. Med. Chem.* **7,** 1773-1789

73. Wenn, S., Lekishvili, T.,Loeschner, C., Sellarajah, S., Prelli, F., Wisniewski, T., Gilber, I. H., and Brown, D. R. (2007) *J. Virol.* **81,** 10729-10741

74. Edwards, R. A., and Woody, R. W. (1979) *Biochemistry* **18,** 5197-5204

75. Ingrosso, L, Ladogana, A., and Pocchiari, M. (1995) *J. Virol*. **69,** 506-508

76. Rudyk, H., Vasiljevic, S., Hennion, R. M., Birkett, C. R., Hope, J., and Gilbert, I. H. (2000) *J. Gen. Virol.* **81,** 1155-1164.

VITA

Name: Joanna Maria Ortiz Alcantara

Address: 2128 TAMU, Texas A&M University,
College Station, TX 77843-2128

Email Address: animousse@hotmail.com

Education: B.S., Pharmaceutical and Biological Chemistry, National Autonomous University of Mexico, 2006

M.S., Biochemistry, Texas A&M University, 2009